Supporting Information

Flexible $Ti_3C_2T_x$/PEDOT:PSS Films with Outstanding Volumetric Capacitance for Asymmetric Supercapacitors

Lu Li[a, b], Na Zhang[c], Mingyi Zhang[b], Xitian Zhang[*, b], Zhiguo Zhang[*, a]

[a] Condensed Matter Science and Technology Institute, Department of Physics, Harbin Institute of Technology, Harbin 150001, People's Republic of China.

[b] Key Laboratory for Photonic and Electronic Bandgap Materials, Ministry of Education, School of Physics and Electronic Engineering, Harbin Normal University, Harbin 150025, People's Republic of China.

[c] Department of Chemistry and Chemical Biology, Cornell University, Ithaca, USA.

[*]Corresponding author: E–mail: xtzhangzhang@hotmail.com (X. T. Zhang)
[*]Corresponding author: E–mail: zhangzhiguo@hit.edu.cn (Z. G. Zhang)

Calculation

The capacitance could be calculated from CV or GCD curves by the following equations.

For specific capacitance (C_m):

From CV curves: $$C_m = \frac{\int I dV}{2 \cdot m \cdot v \cdot \Delta V} \quad (1)$$

Here, C_m is the specific capacitance (F g^{-1}). I is the response current (A), V is the potential vs. reference electrode (V), m is mass (mg), ν is the scan rate (mV s^{-1}), ΔV is the potential window (V).

From GCD curves: $$C_m = \frac{I \cdot \Delta t}{m \cdot \Delta V} \quad (2)$$

Here, C_m is the specific capacitance (F g^{-1}). I is the current (A), Δt is the discharging time (s), m is mass (mg) and ΔV is the potential window (V).

For volumetric capacitance (C_v):

$$C_v = \rho \cdot C_m \quad (3)$$

Here, C_m is the specific capacitance (F g^{-1}), C_v is the volumetric capacitance (F cm^{-3}), and ρ is the electrode density (g cm^{-3}).

Before assembling the ASC, it is necessary to maintain charge balance between positive and negative electrodes. The mass ratio of the negative electrode to the positive electrode was decided based on charge balance theory ($q_+ = q_-$). The charge stored (q) by each electrode depends on the following equation:

$$q = C_m \times \Delta V \times m \quad (4)$$

The volumetric capacitance (C), energy density (E) and power density (P) of the

ASC could be calculated by the following equations.

$$C = \frac{\mathrm{I} \cdot \Delta t}{\mathrm{v} \cdot \Delta V} \tag{5}$$

$$E = \frac{1}{2} C \cdot (\Delta V)^2 \tag{6}$$

$$P = \frac{E}{\Delta t} \tag{7}$$

Here, C is the volumetric capacitance (F cm^{-3}), I is the constant discharge current (A), Δt is the discharging time (s), v is the volume of active materials including the two working electrodes (cm^{-3}), and ΔV is the cell voltage (V).

Table S1. Experimental parameters of the prepared samples.

Sample	$Ti_3C_2T_x$ NSs (mL) (1.5 mg/mL)	PH1000 (μL) (1.5%)	MXene content	Soaked in concentrated H_2SO_4	Density (g/cm^3)
$Ti_3C_2T_x$	10	0	100%	-	3.95
$Ti_3C_2T_x$/P-50	10	50	95.2%	-	3.67
$Ti_3C_2T_x$/P-100	10	100	90.9%	-	3.29
$Ti_3C_2T_x$/P-200	10	200	83.3%	-	3.13
$Ti_3C_2T_x$-H	10	0	-	24 h	3.95
$Ti_3C_2T_x$/P-50-H	10	50	-	24 h	3.92
$Ti_3C_2T_x$/P-100-H	10	100	-	24 h	3.72
$Ti_3C_2T_x$/P-200-H	10	200	-	24 h	3.31

Table S2. The comparison of related experimental results of volumetric capacitance from recent years.

Material	Electrolyte	Volumetric capacitance	Ref.
few-layer $Ti_3C_2T_x$	1M KOH	350 mF/cm^3 at 2 mV/s	1
$Ti_3C_2T_x$ clay	1M H_2SO_4	900 mF/cm^3 at 2 mV/s	2
d-Ti_3C_2/CNT	6M KOH	393 mF/cm^3 at 5 mV/s	3
PPy/ $Ti_3C_2T_x$ films	1M H_2SO_4	1000 mF/cm^3 at 5 mV/s	4
$Ti_3C_2T_x$	1M H_2SO_4	360 mF/cm^3 at 2 mV/s	5
Mixed $Ti_3C_2T_x$/SWCNT	1M H_2SO_4	300 mF/cm^3 at 2 mV/s	5
Sandwich-like $Ti_3C_2T_x$/SWCNT	1M H_2SO_4	390 mF/cm^3 at 2 mV/s	5
Sandwich-like $Ti_3C_2T_x$/OLC	1M H_2SO_4	397 mF/cm^3 at 2 mV/s	5
Sandwich-like $Ti_3C_2T_x$/rGO	1M H_2SO_4	435 mF/cm^3 at 2 mV/s	5
d-Ti_3C_2	1M H_2SO_4	520 mF/cm^3 at 2 mV/s	6
$Ti_3C_2T_x$/PVA	1M KOH	528 mF/cm^3 at 2 mV/s	7
$Ti_3C_2T_x$ hydrogels	3M H_2SO_4	1500 mF/cm^3 at 2 mV/s	8
$Ti_3C_2T_x$/PDDA film	1M KOH	296 mF/cm^3 at 2 mV/s	7
HM treated $Ti_3C_2T_x$	1M H_2SO_4	250 mF/cm^3 at 2 mV/s	9
$Ti_3C_2T_x$/rGO	3M H_2SO_4	1040 mF/cm^3 at 2 mV/s	10
$Ti_3C_2T_x$/P3	1M H_2SO_4	1026 mF/cm^3 at 2 mV/s	11
MnO_x-Ti_3C_2 film	1 M $LiSO_4$	602 mF/cm^3 at 2 mV/s	12
$Ti_3C_2T_x$/P-100-H	**1M H_2SO_4**	**1065 mF/cm^3 at 2 mV/s**	**This work**

Table S3. The comparison of related experimental results from recent years.

Supercapacitor	Energy density (mWh/cm^3)	Power density (mW/cm^3)	Reference
EG/Ti_3C_2 1:3 SC	4.8	40	13
	1.4	1 600	
Ti_3C_2/rGO-5% SC	10.3	74 400	10
MnO_x/ Ti_3C_2 SC	13.6	100	12
	10.5	3 756	
Ti_3C_2// rGO ASC	8.6	200	14
L-s- Ti_3C_2 SC	11	15 000	15
	18	700	
Ti_3C_2 SC	5.48	~1 000	16
	6.1	~100	
Nanoporous Ti_3C_2 film SC	20.7	184.8	17
Ti_3C_2 SC	2.3	159.6	18
	1.3	2 015	
PPy/l-Ti_3C_2 SC	10	500	19
EG SC	4.9	317 000	20
Nanoporous graphene film SC	2.65	20 800	21
GO film//3D-DG@MnO_2	28.2	30 000	22
	16	55 000	
MXene-CNT// RuO_2/CNT yarn	61.6	358	23
$Ti_3C_2T_x$/P-100-H//rGO ASC	**23**	**848**	**This work**
	13	**7659**	

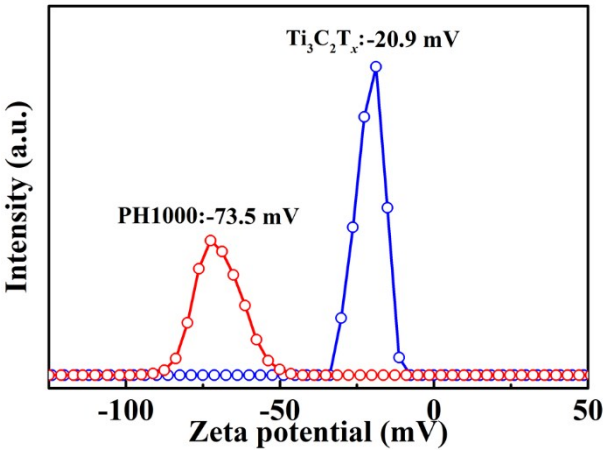

Fig. S1 Zeta potential of $Ti_3C_2T_x$ and PH1000 aqueous solution.

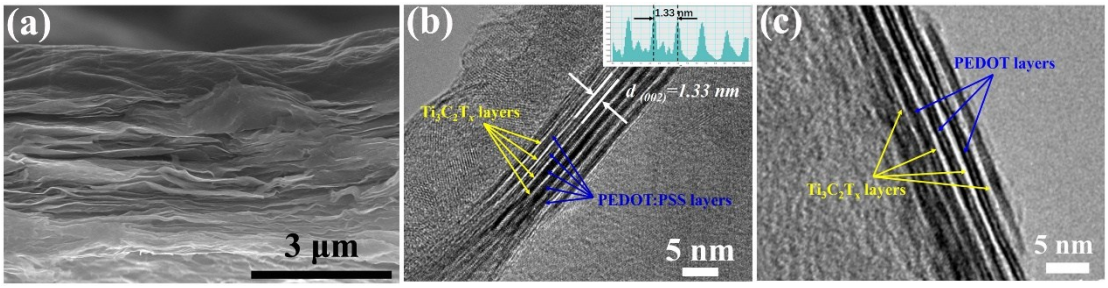

Fig. S2 (a) Cross-section SEM image of $Ti_3C_2T_x$ after H_2SO_4 treatment. (b) HRTEM images of $Ti_3C_2T_x$/P-100 film, inset is profile plot of the calibration for measuring the spacing of $Ti_3C_2T_x$ NSs. (c) Enlarged HRTEM images of $Ti_3C_2T_x$/P-100-H film.

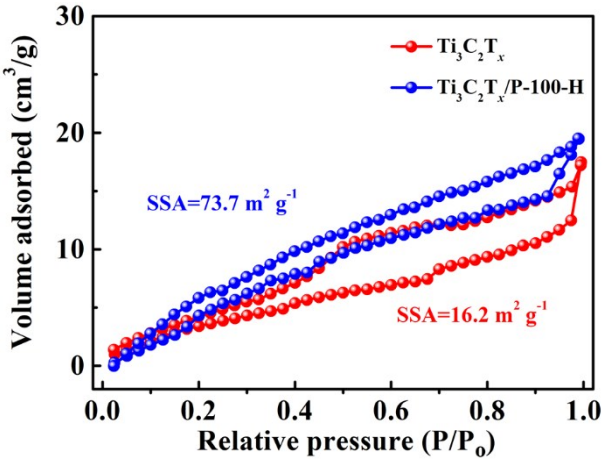

Fig. S3 Nitrogen adsorption and desorption isotherms of $Ti_3C_2T_x$/P-100-H hybrid film and $Ti_3C_2T_x$ film.

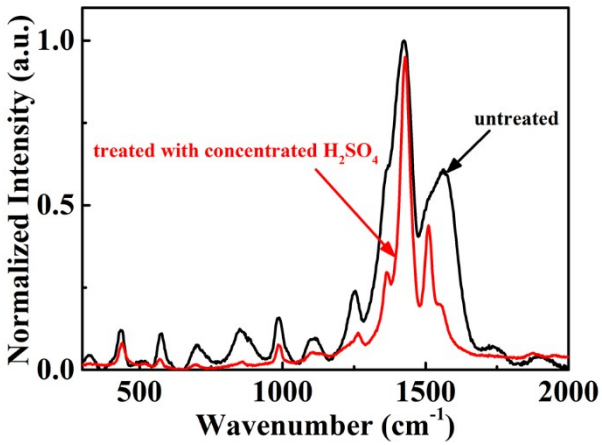

Fig. S4 Raman spectra of PEDOT film before and after concentrated H_2SO_4 treatment.

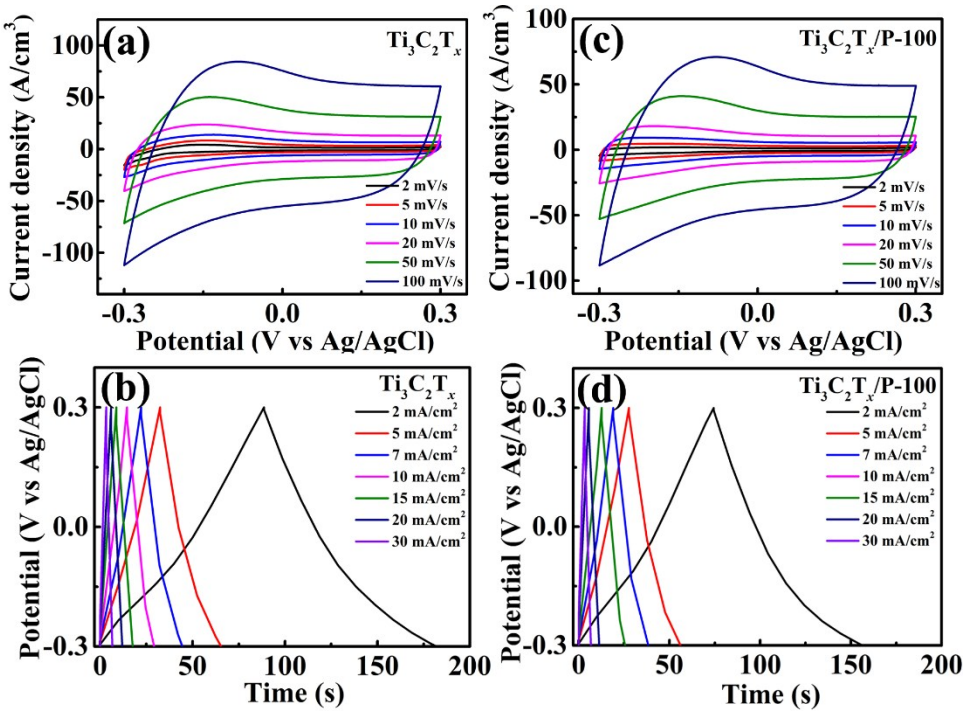

Fig. S5 CV curves of (a) $Ti_3C_2T_x$ and (c) $Ti_3C_2T_x$/P-100 electrode at different scan rates, GCD curves of (b) $Ti_3C_2T_x$ and (d) $Ti_3C_2T_x$/P-100 electrode at different current densities.

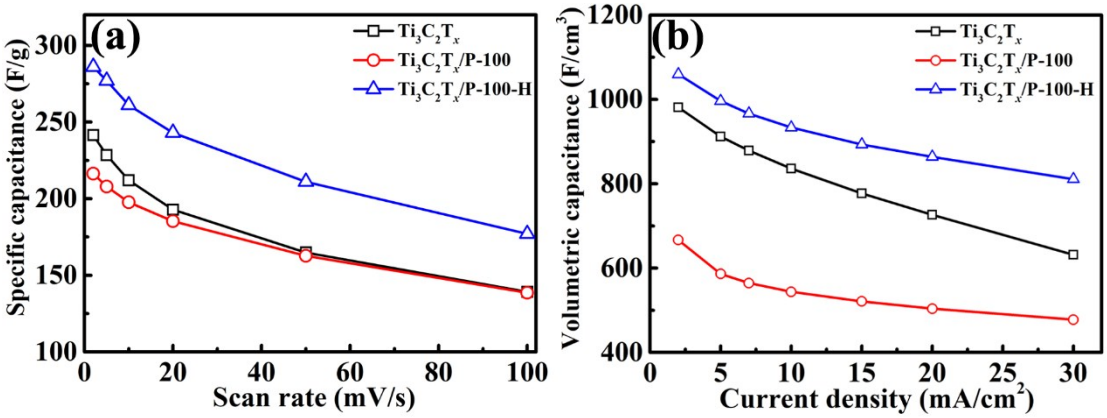

Fig. S6 (a) Specific capacitance of the as-prepared hybrid film electrodes as a function of scan rate. (b) Volumetric capacitance of the as-prepared hybrid film electrodes as a function of current density.

The relationships of specific capacitance as a function of scan rates for the as-prepared samples are shown Fig. S6(a). The pure $Ti_3C_2T_x$ film electrode showed the specific capacitance of 241 F g^{-1} at 2 mV s^{-1} and a rate performance of 58 % as the scan rate increases to 100 mV s^{-1}. After mixing PH1000 with $Ti_3C_2T_x$ to form the $Ti_3C_2T_x$/P-100 film, the specific capacitance decreases dramatically to 216 F g^{-1} at 2 mV s^{-1}. However, after treated by concentrated H_2SO_4, the specific capacitance of $Ti_3C_2T_x$/P-100-H film electrode is significantly improved to 286 F g^{-1} at 2 mV s^{-1} and the capacitance retention is 62% after increasing the scan rate by 50 times.

The volumetric capacitance calculated from GCD curves of the as-prepared samples are shown Fig. S6(b). Compared with the pure $Ti_3C_2T_x$ film electrode with volumetric capacitance of 980 F cm^{-3} at 2 mA cm^{-2}, the $Ti_3C_2T_x$/P-100 film showed a decreased volumetric capacitance of 667 F cm^{-3}. However, after concentrated H_2SO_4 treatment, the volumetric capacitance of $Ti_3C_2T_x$/P-100-H film electrode is significantly improved to 1060 F cm^{-3}.

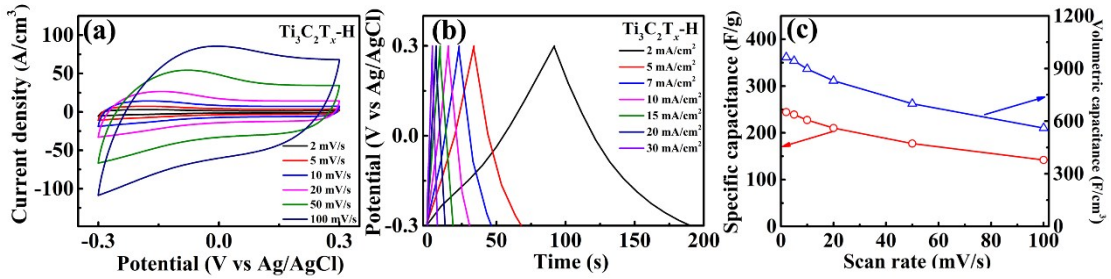

Fig. S7 (a) CV curves and (b) GCD curves of $Ti_3C_2T_x$-H electrode at different current densities, (c) Volumetric capacitance and specific capacitance of $Ti_3C_2T_x$-H electrode as a function of scan rate.

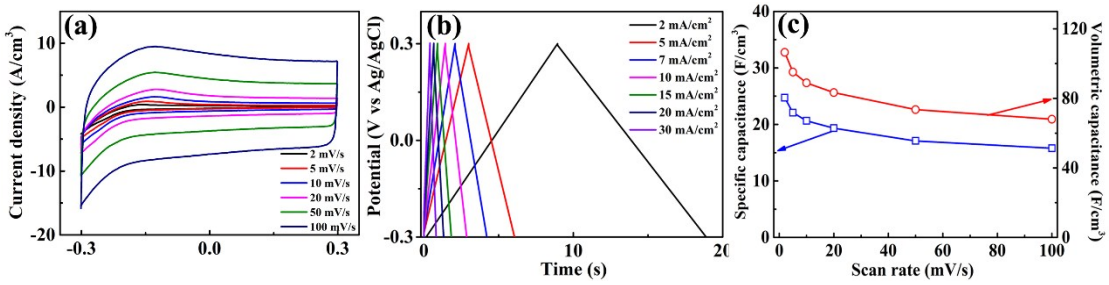

Fig. S8 (a) CV curves of P-H electrode at different scan rates, (b) GCD curves of P-H electrode at different current densities, (c) Volumetric capacitance and specific capacitance of P-H film electrode as a function of scan rate.

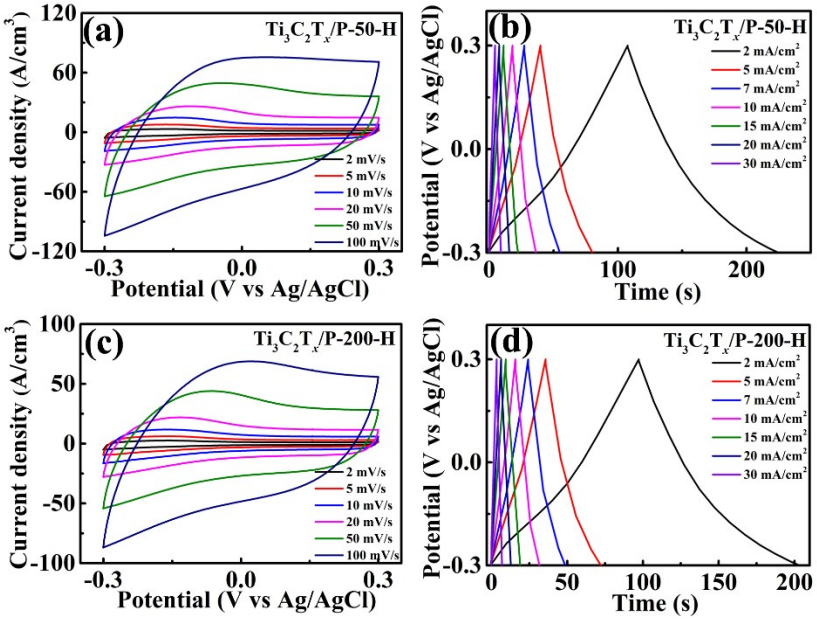

Fig. S9 CV curves of (a) $Ti_3C_2T_x$/P-50-H and (c) $Ti_3C_2T_x$/P-200-H electrode at different scan rates, GCD curves of (b) $Ti_3C_2T_x$/P-50-H and (d) $Ti_3C_2T_x$/P-200-H electrode at different current densities.

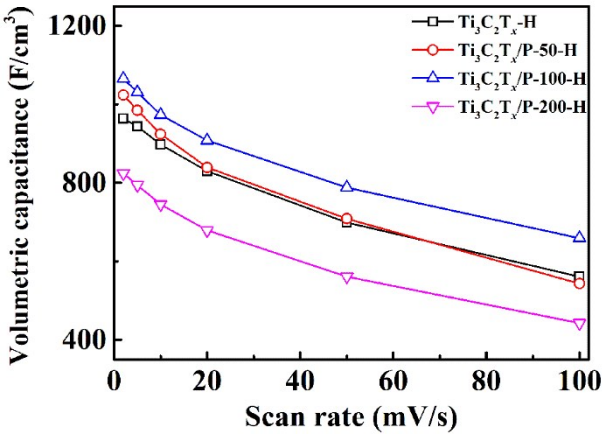

Fig. S10 Volumetric capacitance of the as-prepared hybrid film electrodes as a function of scan rate.

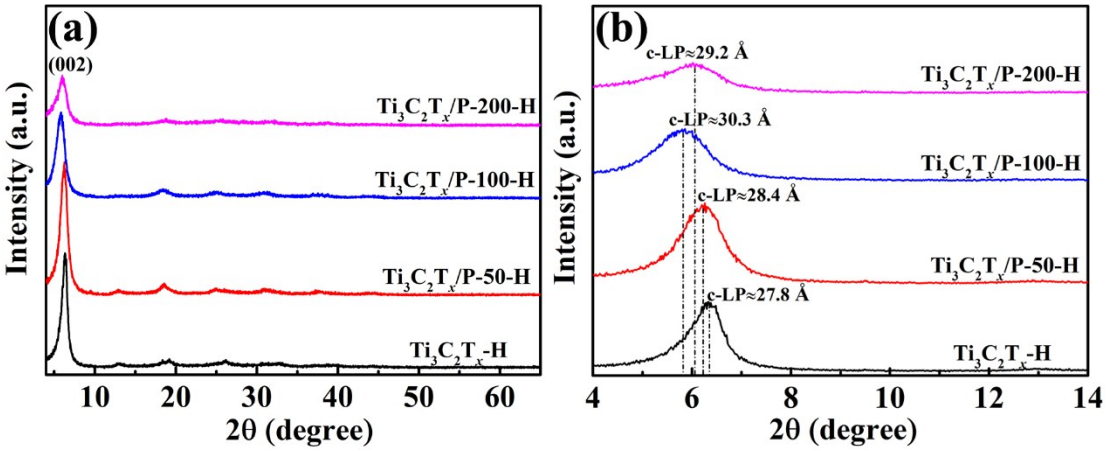

Fig. S11 (a) XRD patterns of $Ti_3C_2T_x$-H, $Ti_3C_2T_x$/P-50-H, $Ti_3C_2T_x$/P-100-H and $Ti_3C_2T_x$/P-200-H and (b) the corresponding enlarged XRD patterns.

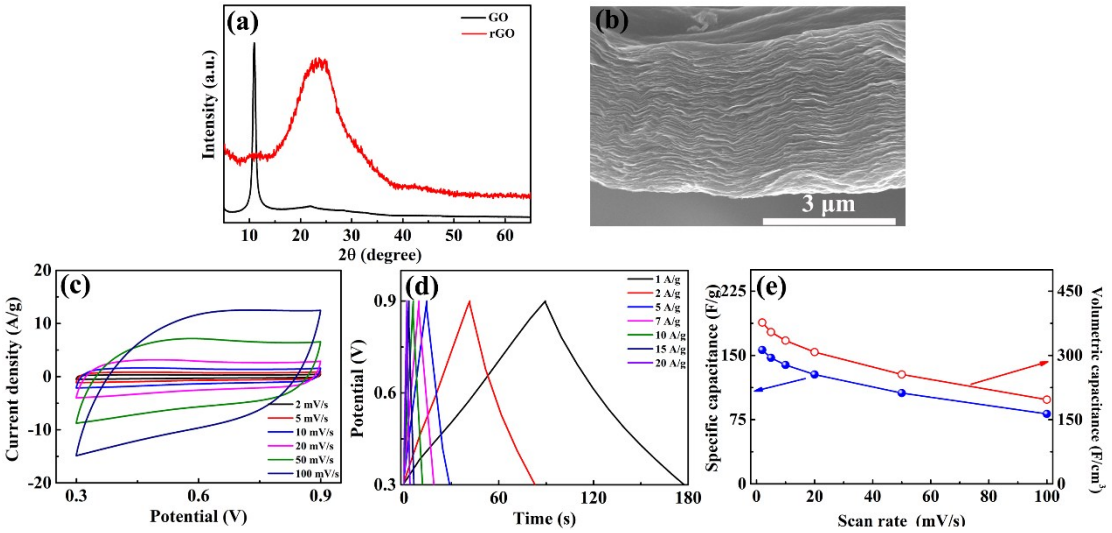

Fig. S12 (a) XRD patterns of GO and rGO film, (b) cross-section SEM image of rGO film, (c) CV curves of rGO film electrode at different scan rates, (d) GCD curves of rGO film electrode at different current densities, (c) Volumetric capacitance and specific capacitance of rGO film electrode as a function of scan rate.

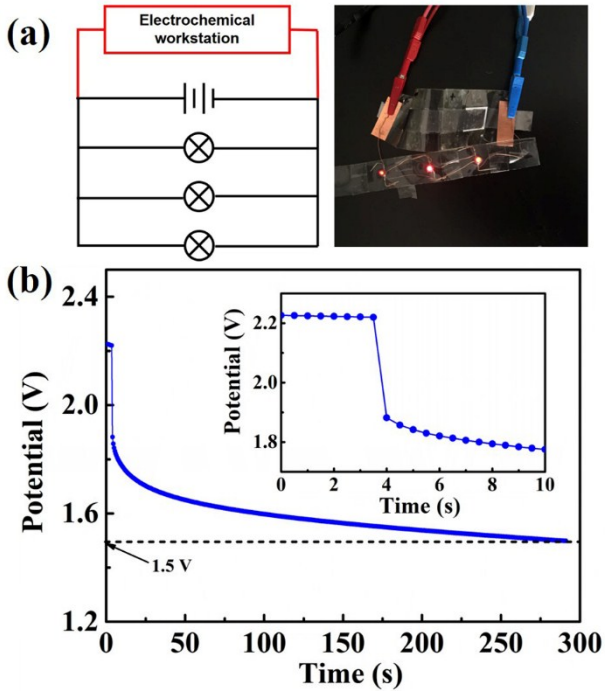

Fig. S13 (a) The equivalent circuit diagram and physical diagram of OCV test, (b) OCV curve of the serial-connected ASCs, the inset is the enlarged OCV curve.

The discharge curve of the serial-connected ASCs when connected to the LEDs is obtained by OCV test as shown in Fig. S13. Fig. S13 is added in the supplementary. The equivalent circuit diagram and physical diagram of OCV test is shown in Fig. S13a. The electrochemical workstation is in parallel with the ASCs. Once the LEDs are connected to the circuit, the voltage drops significantly at the 4th second, as shown in the inset in Fig. S13b. When the voltage is less than 1.5V, the LEDs are extinguished. Thus, the serial-connected ASCs could drive the luminous band for about five minutes.

Notes and references

1. M. R. Lukatskaya, O. Mashtalir, C. E. Ren, Y. D. Agnese, P. Rozier, P. L. Taberna, M. Naguib and P. Simon, *Science*, 2013, **341**, 1502.
2. M. Ghidiu, M. R Lukatskaya, M. Q. Zhao, Y. Gogotsi and M. W. Barsoum, *Nature*, 2014, **516**, 78.
3. P. T. Yan, R. J. Zhang, J. Jia, C. Wu, A. G. Zhou, J. Xu and X. S. Zhang, *J. Power Sources.*, 2015, **284**, 38
4. M. Boota, B. Anasori, C. Voigt, M. Q. Zhao, M. W. Barsoum and Y. Gogotsi, *Adv. Mater.*, 2016, **28**, 1517.
5. M. Q. Zhao, C. E. Ren, Z. Ling, M. R. Lukatskaya, C. F. Zhang, K. L. V. Aken, M. W. Barsoum and Y. Gogotsi, *Adv. Mater.*, 2015, **27**, 339.
6. Y. Dall'Agnese, M. R. Lukatskaya, K. M. Cook, P. L. Taberna, Y. Gogotsi and P. Simon, *Electrochem. Commun.*, 2014, **48**, 118.
7. Z. Ling, C. E. Ren, M. Q. Zhao, J. Yang, J. M. Giammarco, J. S. Qiu, M. W. Barsoum and Y. Gogotsi, *PNAS*, 2014, **111**, 16676.
8. M. R. Lukatskaya, S. Kota, Z. F. Lin, M. Q. Zhao, N. Shpigel, M. D. Levi, J. Halim, P. L. Taberna, M. W. Barsoum, P. Simon and Y. Gogotsi, *Nat. Energy.*, 2017, **2**, 17105.
9. O. Mashtalir, M. R. Lukatskaya, A. I. Kolesnikov, E. Raymundo-Piñero, M. Naguib, M. W. Barsouma and Y. Gogotsi, *Nanoscale*, 2016, **8**, 9128.
10. J. Yan, C. E. Ren, K. Maleski, C. B. Hatter, B. Anasori, P. Urbankowski, A. Sarycheva and Y. Gogotsi, *Adv. Funct. Mater.*, 2017, **27**, 1701264.

11. M. Boota, M. Pasini, F. Galeotti, Wi. Porzio, M. Q. Zhao, J. Halim and Y. Gogotsi, *Chem. Mater.*, 2017, **29**, 2731.

12. Y. P. Tian, C. H. Yang, W. X. Que, X. B. Liu, X. T. Yin and L. B. Kong, *J. Power Sources*, 2017, **359**, 332.

13. H. Y. Li, Y. Hou, F. X. Wang, M. R. Lohe, X. D. Zhuang, L. Niu and X. L. Feng, *Adv. Energy Mater.*, 2016, **28**, 1601847.

14. C. Couly, M. Alhabeb, K. L. Van Aken, N. Kurra, L. Gomes, A. M. Navarro-Suárez, B. Anasori, H. N. Alshareef and Y. Gogotsi, *Adv. Electron. Mater.*, 2018, **4**, 1700339.

15. Y. Y. Peng, B. Akuzum, N. Kurra, M. Q. Zhao, M. Alhabeb, B. Anasori, E. C. Kumbur, H. N. Alshareef, M. D. Ger and Y. Gogotsi, *Energy Environ. Sci.*, 2016, **9**, 2847.

16. H. B. Hu and T. Hua, *J. Mater. Chem. A*, 2017, **5**, 19639.

17. Z. M. Fan, Y. S. Wang, Z. M. Xie, X. Q. Xu, Y. Yuan, Z. J. Cheng and Y. Y. Liu, *Nanoscale*, 2018, **10**, 9642.

18. P. Li, W. H. Shi, W. X. Liu, Y. F. Chen, X. L. Xu, S. F. Ye, R. L. Yin, L. Zhang, L. X. Xu and X. H. Cao, *Nanotechnology*, 2018, **29**, 445401.

19. M. S. Zhu, Y. Huang, Q. H. Deng, J. Zhou, Z. X. Pei, Q. Xue, Y. Huang, Z. F. Wang, H. F. Li, Q. Huang and C. Y. Zhi, *Adv. Energy Mater.*, 2016, **6**, 1600969.

20. Z. S. Wu, Y. J. Zheng, S. H. Zheng, S. Wang, C. L. Sun, K. Parvez, T. Ikeda, X. H. Bao, K. Müllen and X. L. Feng, *Adv. Mater.*, 2017, **29**, 1602960.

21. K. Q. Qin, J. L. Kang, J. J. Li, E. Z. Liu, C. S. Shi, Z. J. Zhang, X. X. Zhang and

N. Q. Zhao, *Nano energy*, 2016, **24**, 158.

22. K. Q. Qin, E. Z. Liu, J. J. Li, J. L. Kang, C. S. Shi, C. N. He, F. He and N. Q. Zhao, *Adv. Energy Mater.*, 2016, **6**, 1600755.

23. Z. Y. Wang, S. Qin, S. Y. Seyedin, J. Z. Zhang, J. T. Wang, A. Levitt, N. Li, C. Haines, R. O. Robles, W. W. Lei, Y. Gogotsi, R. H. Baughman and J. M. Razal, *Small*, 2018, **14**, 1802225.